HHS Public Access

Author manuscript

Proc SPIE Int Soc Opt Eng. Author manuscript; available in PMC 2019 October 10.

Published in final edited form as:

Proc SPIE Int Soc Opt Eng. 2019 March ; 10948: . doi:10.1117/12.2512949.

Consideration of Cerebrospinal Fluid Intensity Variation in Diffusion Weighted MRI

Colin B. Hansen[a], **Vishwesh Nath**[a], **Allison E. Hainline**[b], **Kurt G. Schilling**[c], **Prasanna Parvathaneni**[d], **Roza G. Bayrak**[a], **Justin A. Blaber**[d], **Owen Williams**[g], **Susan Resnick**[g], **Lori Beason-Held**[g], **Okan Irfanoglu**[e], **Carlo Pierpaoli**[e], **Adam W. Anderson**[c,f], **Baxter P. Rogers**[c,f], **Bennett A. Landman**[a,c,d,f]

[a]Computer Science, Vanderbilt University, Nashville, TN, USA

[b]Biostatistics, Vanderbilt University, Nashville, TN, USA

[c]Department of Radiology and Radiological Sciences, Vanderbilt University Medical Center, Nashville, TN USA

[d]Electrical Engineering, Vanderbilt University, Nashville, TN, USA

[e]National Institute of Biomedical Imaging and Bioengineering, Bethesda MD USA

[f]Department of Biomedical Engineering, Vanderbilt University, Nashville, TN USA

[g]National Institutes of Health, Bethesda, MD

Abstract

Diffusion weighted MRI (DW-MRI) depends on accurate quantification signal intensities that reflect directional apparent diffusion coefficients (ADC). Signal drift and fluctuations during imaging can cause systematic non-linearities that manifest as ADC changes if not corrected. Here, we present a case study on a large longitudinal dataset of typical diffusion tensor imaging. We investigate observed variation in the cerebral spinal fluid (CSF) regions of the brain, which should represent compartments with isotropic diffusivity. The study contains 3949 DW-MRI acquisitions of the human brain with 918 subjects and 542 with repeated scan sessions. We provide an analysis of the inter-scan, inter-session, and intra-session variation and an analysis of the associations with the applied diffusion gradient directions. We investigate a hypothesis that CSF models could be used in lieu of an interspersed minimally diffusion-weighted image (b0) correction. Variation in CSF signal is not largely attributable to within-scan dynamic anatomical changes (3.6%), but rather has substantial variation across scan sessions (10.6%) and increased variation across individuals (26.6%). Unfortunately, CSF intensity is not solely explained by a main drift model or a gradient model, but rather has statistically significant associations with both possible explanations. Further exploration is necessary for CSF drift to be used as an effective harmonization technique.

Keywords

Diffusion; CSF; BLSA; variation

1. INTRODUCTION

Vos et al. recently reviewed the effectiveness of using minimally weighted images ("b0's") interspersed throughout a scan to correct temporal instability in scanner systems [1-3] and this was extended to spatially temporal models [4]. In addition, correcting for non-linearities in the gradient fields of the magnetic coils can be accomplished through empirical field mapping techniques [5, 6]. However, these corrections are not viable for datasets that were acquired before these techniques became widely available. Cerebral spinal fluid (CSF) can be used to observe trends in signal intensity as it is known to be isotropic. We present a case study on a large longitudinal dataset and examine variation in the CSF regions of the human brain (Figure 1, Figure 2, and Table 1).

2. DATA

Herein, we consider a large longitudinal dataset comprised of 3949 MRI brain acquisitions of 918 subjects. Subjects have repeated DW-MRI acquisitions in each session, and 542 subjects have repeat sessions at later dates. All data were acquired after informed consent under institutional review board and accessed in de-identified form. Each session included a T1-weighted structural MP-RAGE (number of slices=170, voxel size=1mm×1mm×1.2mm, reconstruction matrix=256×256, flip angle=8 degrees and TR/TE=6.5ms/3.1ms) and two diffusion acquisitions. Each diffusion acquisition consists of an initial b0 image and thirty-two diffusion weighted volumes all with a b-value of 700 s/mm^2 (number of gradients=32, number of b0 images=1, TR/TE=7454/75 ms, number of slices=70, voxel size=0.81×0.81×2.2 mm^3, reconstruction matrix=320×320, acquisition matrix=116×115, field of view=260×260 mm, flip angle=90°). Susceptibility correction [7] and eddy current correction [8] techniques are applied to the diffusion data as a preprocessing step as well as b0 signal normalization. The MP-RAGE was segmented with the BrainCOLOR protocol (Neuromorphometrics, Inc., Somerville, MA) using hierarchical non-local spatial STAPLE [9]. For each 3D volume in a scan, the median signal is computed within the co-registered (FSL flirt[10]) regions of interest (ROI) from the BrainCOLOR segmentation defined over three CSF filled regions in the brain: the right lateral ventricle, left lateral ventricle, and third ventricle.

Variation

Figure 1 shows qualitatively the variation in the left and right lateral ventricles in a single scan. In Figure 2, the median normalized signal (i.e., diffusion weighted intensity divided by the minimally weighed reference) for all scans in the three ROIs is shown over the course of the thirty-two acquired diffusion volumes after the first median value of each scan has been subtracted to ensure all timeseries have the same starting position of zero. From this the variation across all scans can be seen at certain volumes especially in the left and right lateral ventricles. In Table 1, the average standard deviation for all ROIs is shown for intra-session data, inter-session data, and for inter-subject data. The standard deviation nearly triples from intra-session to inter-session and again at least doubles from inter-session to inter-subject. The relatively low standard deviation within in a session and higher standard deviation across all sessions for a subject indicates that the variation is not only an effect of

anatomical differences. The steady increase in standard deviation from intra-session to inter-session to inter-subject indicates that the effect is static.

Modes of Variation

Figure 3 shows the contribution of variation from the principle components of the median signals as well as the cumulative variation from the most contribution component to the least for each ROI. It can be seen that almost ninety percent of the variance can be attributed to the first three components indicating that an appropriate correction model would be able to reduce this variance. In Figure 4, the first three components are normalized and plotted. Figure 5 shows the same data from Figure 2 represented as a scatter plot, but now the color of the point represents the value of the corresponding gradient direction. In the right and left lateral ventricles, it can be seen that the volumes with the most variation are either acquired with the gradient taken along the y or z direction and the volumes with the least variation are acquired with the gradient taken along the x direction. In addition, it seems that the sharp decreases in the plot of component one in Figure 4 correlates with the volumes at which the gradient is taken in the y direction as seen in Figure 5.

3. MODELS

To capture the variability in the signal, we examine five models: two linear models and three non-linear models, which will be referred to as models one through five. This section outlines the basis function used to approximate the signal through regression.

Linear Model

The linear model approximates the apparent diffusion coefficient (ADC) as a constant and attributes variation to temporal drift and baseline sensitivity to applied gradient direction. For example, these effects could be associated with directional flow related effects. The first linear model is defined by:

$$S(n,X) = d_1 s0 + d_2 n + d_3 n^2 + d_4 x + d_5 y + d_6 z + d_7 xy + d_8 xz + d_9 yz + d_{10} x^2 + d_{11} y^2 + d_{12} z^2 \quad (1)$$

where is the normalized signal, $s0$ is the normalized signal at the first volume, n is the volume index, and x, y, and z correspond to the vector X that defines the gradient direction (b-vector). The coefficients are defined by d_i.

Log Model

The logarithmic model (“log model”) captures potential changes in ADC related to applied gradient direction. The baseline signal intensity is assumed to be constant. For example, these effects could be related to imaging gradient alterations in b-vector or nonidealities in applied gradients. The log model is defined by:

$$\log(S) = d_1\log(s0) + d_2x + d_3y + d_4z + d_5xy + d_6xz + d_7yz + d_8x^2 + d_9y^2 + d_{10}z^2 \quad (2)$$

Simple Exponential Model

The third model is a simple concatenation of both prior models, while dropping temporal baseline drift (as it was not found to be significant, see below). The first non-linear model is defined by:

$$S_L = d_1s0 + d_2x + d_3y + d_4z \quad (3)$$

$$S_e = e^{-d_5s0 - d_6x - d_7y - d_8z} \quad (4)$$

$$S = S_LS_e \quad (5)$$

Where S_L is the linear portion of the model S_e and is the exponential portion of the model.

Cross-term Exponential Model

The second non-linear model expands the third model to evaluate potential interactions between the gradients:

$$S_L = d_1s0 + d_2x + d_3y + d_4z + d_5xy + d_6xz + d_7yz \quad (6)$$

$$S_e = e^{-d_8s0 - d_9x - d_{10}y - d_{11}z - d_{12}xy - d_{13}xz - d_{14}yz} \quad (7)$$

$$S = S_LS_e \quad (8)$$

Squared Exponential Model

The fourth non-linear model expands on the third model with non-linear terms for the x and y gradient direction but neglects cross terms due to limited statistical power:

$$S_L = d_1s0 + d_2x + d_3y + d_4z + d_5x^2 + d_6y^2 \quad (9)$$

$$S_e = e^{-d_7 s0 - d_8 x - d_9 y - d_{10} z - d_{11} x^2 - d_{12} y^2} \quad (10)$$

$$S = S_L S_e \quad (11)$$

Model Analysis

Each model was fit to the median signal in the left and right lateral ventricles from each scan. The significance values associated with each term of the models are visualized for each scan in Figure 6. In the linear and log model, the $s0$, yz, and quadratic terms were the most significant. In the simple and cross-term model, the $s0$, y, z, e^{s0}, e^{y}, and e^{z} terms were the most significant. In the squared exponential model, only the $s0$, z, e^{s0}, and e^{z} terms were significant in most of the fits. In the linear model, we can see that the terms representing the index of the volume are insignificant which indicates that temporal affects are not causing the high variation. An estimation for the median signal of each scan was generated using the coefficients learned from each regression and the total root mean squared error (rmse) is shown in Table 2 for each method. In terms of accurately estimating the signal, the squared exponential model performed the best by a small margin over the other models. Table 2 also shows the mean R^2 and mean adjusted R^2 for each model. The cross-term exponential model had the highest R^2 while the squared exponential model had the highest adjusted R^2.

4. CONCLUSION

The isotropic nature of CSF has allowed us to look at the variation of the signal which may be indicative of the variation within surrounding areas or even the whole brain. With few modes of variation, a viable model should be able to estimate the median signal with few variables being utilized as basis functions. Our results show that using the values of the b-vector to fit a model to each scan's signal over time allows for fairly accurate estimations. However, it is not clear if there is a strong correlation between the variation in the white matter of the brain and the variation in the CSF. If there is a strong positive correlation between the median signal in the CSF and the surrounding white matter regions in the brain, the estimated signal could be used to correct the variation in the same manner as the b0 drift correction as proposed by Vos et al [3]. Unfortunately, the CSF does not appear to provide a clear reference tissue. Yet, the variations are highly structured, dependent on diffusion weighting direction, and may provide useful anatomical metrics with additional biophysical modeling.

ACKNOWLEDGEMENTS

This work was supported by R01EB017230 (Landman). This work was conducted in part using the resources of the Advanced Computing Center for Research and Education at Vanderbilt University, Nashville, TN. This project was supported in part by the National Center for Research Resources, Grant UL1 RR024975-01, and is now at the National Center for Advancing Translational Sciences, Grant 2 UL1 TR000445-06. This research was conducted with the support from Intramural Research Program, National Institute on Aging, NIH. The content is solely the responsibility of the authors and does not necessarily represent the official views of the NIH.

REFERENCES

1. Thesen S, Kruger G, and Muller E. Absolute correction of B0 fluctuations in echo-planar imaging. in Proceedings of the International Society of Magnetic Resonance in Medicine 2003.
2. Benner T, et al., Real-time RF pulse adjustment for B0 drift correction. Magnetic resonance in medicine, 2006 56(1): p. 204–209. [PubMed: 16767763]
3. Vos SB, et al., The importance of correcting for signal drift in diffusion MRI. Magnetic resonance in medicine, 2017 77(1): p. 285–299. [PubMed: 26822700]
4. Hansen Colin B., et al., Characterization and Correlation of Signal Drift in Diffusion Weighted MRI. Magnetic Resonance Imaging: An International Journal of Basic Research and Clinical Applications. Submitted 7 2018.
5. Bammer R, et al., Analysis and generalized correction of the effect of spatial gradient field distortions in diffusion-weighted imaging. Magnetic Resonance in Medicine: An Official Journal of the International Society for Magnetic Resonance in Medicine, 2003 50(3): p. 560–569.
6. Rogers BP, et al. Phantom-based field maps for gradient nonlinearity correction in diffusion imaging. in Medical Imaging 2018: Physics of Medical Imaging. 2018 International Society for Optics and Photonics.
7. Andersson JL, Skare S, and Ashburner J, How to correct susceptibility distortions in spin-echo echo-planar images: application to diffusion tensor imaging. Neuroimage, 2003 20(2): p. 870–888. [PubMed: 14568458]
8. Andersson JL and Sotiropoulos SN, An integrated approach to correction for off-resonance effects and subject movement in diffusion MR imaging. Neuroimage, 2016 125: p. 1063–1078. [PubMed: 26481672]
9. Asman AJ and Landman BA, Hierarchical performance estimation in the statistical label fusion framework. Med Image Anal, 2014 18(7): p. 1070–81. [PubMed: 25033470]
10. Smith SM, et al., Advances in functional and structural MR image analysis and implementation as FSL. Neuroimage, 2004 23 Suppl 1: p. S208–19. [PubMed: 15501092]

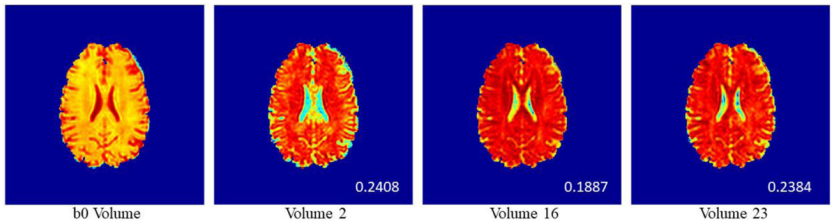

Figure 1.

A slice from the b0 and three diffusion weighted direction of a single scan are shown with logarithmic intensity (a.u.). In the lower right-hand corner of the median intensity of the diffusion weighted volumes within the left lateral ventricle is shown. Note the variation of up to 28% in absolute intensity.

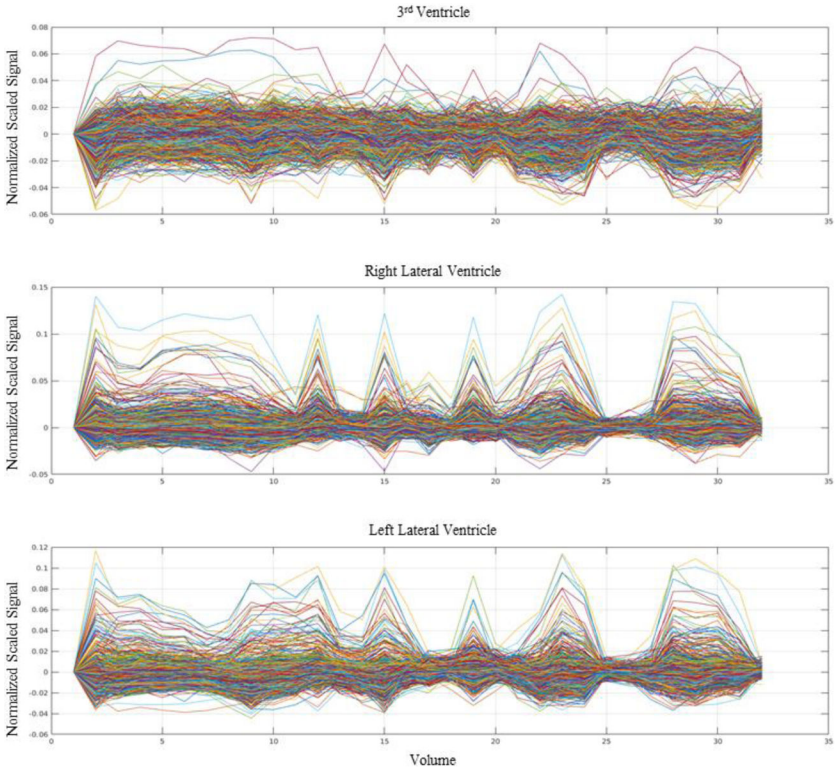

Figure 2.

All median signals for three CSF regions in the brain for 3949 scans, with each line corresponding to a single scan. From top to bottom the rows correspond to the 3rd ventricle, the right lateral ventricle, and the left lateral ventricle. The median signal has been normalized and scaled so that all start at the same point. Note the wide range of signal variation and the visually clear dependence on gradient direction.

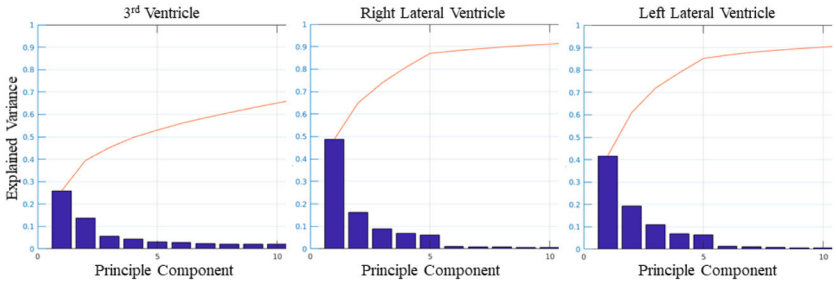

Figure 3.

Here we see the explained variance for the principle components for the median signal for all scans. From left to right the plot corresponds to the 3rd ventricle, right lateral ventricle, and left lateral ventricle. This shows that most of the variance is explained by the first 3 modes of variation.

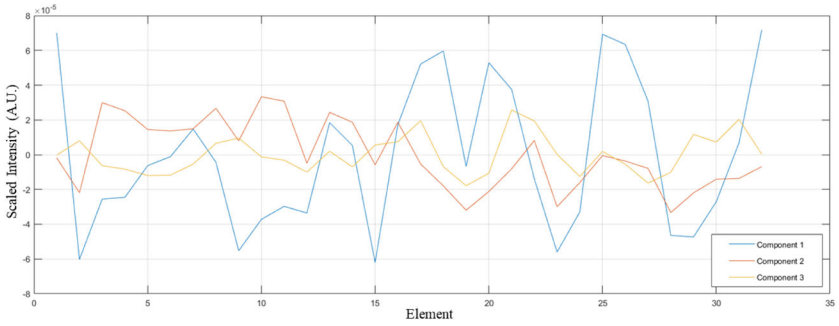

Figure 4.

This plot shows the first three principle components. Note the lack of low frequency temporal drift.

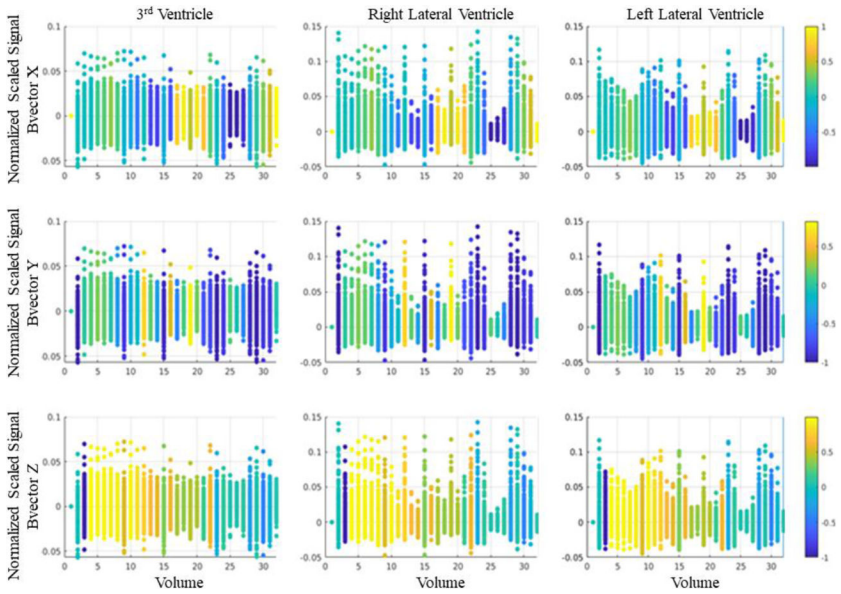

Figure 5.

Each row corresponds to a b-vector (x, y, and z from top to bottom) and each column corresponds to a CSF region (3rd, right lateral, left lateral, from left to right). Each represents the same data from figure 1, but the color represents the value of the b-vector at that volume. This shows that as the variation in the data increases as the gradient is taken in the y and z directions.

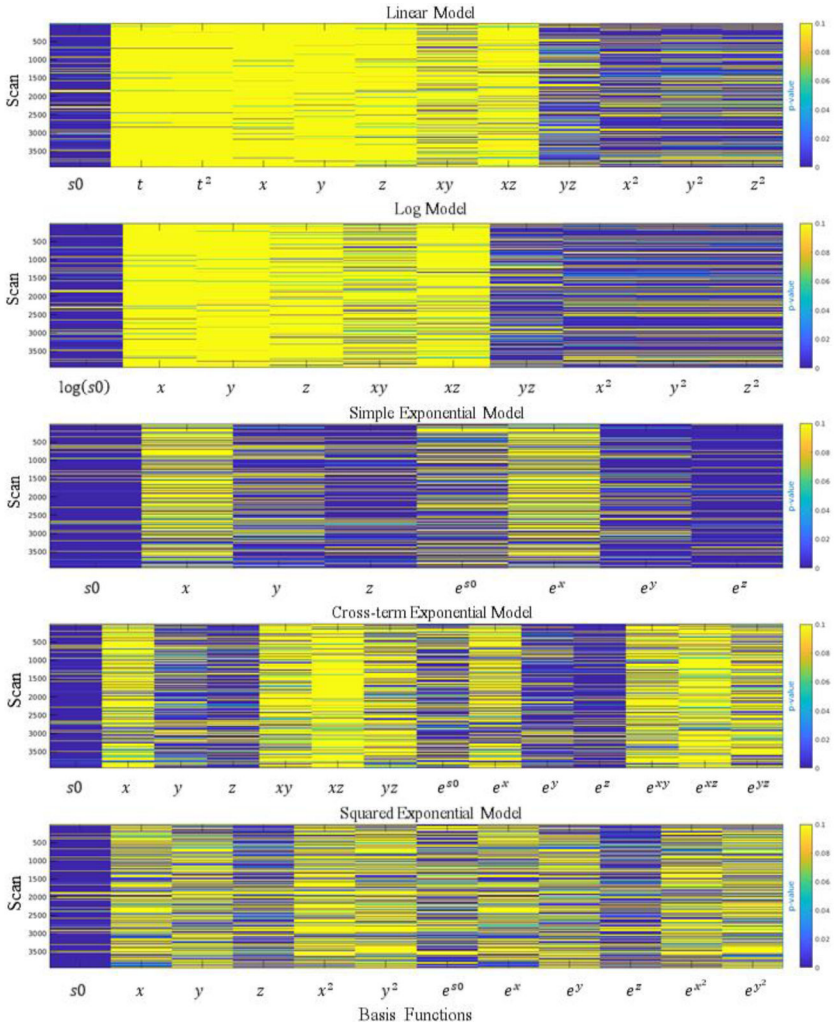

Figure 6.

Each row corresponds to a model used to capture the variance in the left and right lateral ventricles. From top to bottom the models are the linear model, log model, simple exponential model, cross-term exponential model, and squared exponential model. Each row in the images represents p-values of the coefficients from the fitting the model to the median signal. Each column represents one of the terms that were used as the basis functions for the models.

Table 1.

The median standard deviation for all volumes within each session, across all sessions for all subjects, and across all subjects. The percentage of that value with regards to the median signal for all data is also shown. The 3rd column shows the size of the data and the last column shows the p-value of the data against the intra-session data.

Data	Median SD	Percent of Median Signal	N	p-value against Intra-session
Intra-session CSF	0.0029	3.59	1954	N/A
Inter-session CSF	0.0086	10.60	542	< 0.001
Inter-subject CSF	0.0216	26.59	3949	< 0.001

Table 2.

The sum of the root mean squared error between the estimated median signal and the true median signal, the mean R^2, and mean adjusted R^2 for all models for all scans.

Model	Total RMSE	Mean R^2	Mean Adjusted R^2
Linear	10.591	0.797	0.755
Log	10.666	0.794	0.759
Simple Exponential	11.991	0.753	0.722
Cross-term Exponential	10.199	0.818	0.770
Squared Exponential	9.859	0.817	0.779